A quick and selective rhodamine based "smart probe" for "signal-on" optical detection of Cu^{2+} and Al^{3+} in water, cell imaging, computational studies and solid state analysis

Abhishek Rai‡[a], Alok Kumar Singh‡[b], Kamini Tripathi[a], Avinash Kumar Sonkar[a], Brijesh Singh Chauhan[c], S. Srikrishna[c], Tony D. James*[d] and Lallan Mishra*[a]

[a]*Department of Chemistry, Institute of Science, Banaras Hindu University,Varanasi, India.*

[b]*Department of Applied Chemistry, Babasaheb Bhimrao Ambedkar University, Lucknow, India.*

[c]*Department of BioChemistry, Institute of Science, Banaras Hindu University, Varanasi, India*.

[d]*Department of Chemistry, University of Bath, Bath, BA2 7AY U.K*

‡These authors contributed equally to this work.

Abstract

A novel rhodamine hydrazone **1** has been synthesized by the condensation of rhodamine B hydrazide with allylsalicylaldehyde and has been fully characterized using various physicochemical techniques including single crystal XRD. Probe **1** can detect Cu^{2+} and Al^{3+} ions in aqueous media and displays a turn-on response in absorbance with a high degree of selectivity amongst other common interfering analytes. Al^{3+} ions lead to fluorescence enhancementby the opening of the spirolactum ring resulting in chelation enhanced fluorescence. DFT and TDDFT calculations support the experimental results. The **1**-Al^{3+} ensemble acts as secondary sensor for pyrophosphate anion due to metal ion induced decomplexation resulting in a low detection limit. Probe **1** can be utilized for bio imaging and displays morphological transformations from crystalline to amorphous state with associated color changes due to mechanical switching. In the solid state, probe **1** displays distinct color changes with emission at different wavelengths in particular Al^{3+} and Hg^{2+}result in a red shift of the CIE-diagram. While the band gap of probe **1**can be tuned from 2.08 eV to 1.60 eV.Probe **1** meets many real-world-challenges in that it is prepared using simple synthetic methods, produces fast and distinct response towards multiple-ions, observed by the "naked eye" in solution and on a TLC plate, and can be exploited for binary data storage.

*Corresponding authorE mail: *t.d.james@bath.ac.uk*, *lmishrabhu@yahoo.co.in*, Tel: +91-542-6702449,Fax: +91-542-2368174

1. Introduction

Chemosensors suitable for real-time applications, with high selectivity and low detection limit for biologically and environmentally relevant metal ions remains an important challenge. Additionally, chemosensors capable of multiple ion sensing are particularly suitable for practical applications [1-3].

The high absorption coefficient, elevated fluorescence quantum yield, long absorption and emission wavelengths, simple synthetic methodology and ability to exhibit "naked-eye" detection makes rhodamine an extraordinary candidate for chemosensor development. Classically, rhodamine derivatives are colorless and non-fluorescent owing to the closed spirolactam ring structure. The interaction with a particular metal ion opens the spirolactam ring resulting in a change of color and increase in fluorescence [4]. Recently, several rhodamine-based probes have been developed for the selective recognition of Hg^{2+}, Cu^{2+}, Fe^{3+} and Al^{3+} [5-14] in solution, however, the simultaneous detection of multiple ions such as Cu^{2+} and Al^{3+} by a single probe are still limited [15-16].

Copper is the third most abundant essential trace element in the human body and plays an important role in a number of physiological processes [17]. High levels of copper causes gastrointestinal disturbances, even after a short period of exposure, while its long term exposure can affect the liver or kidneys [18]. Copper ions are associated with serious diseases, such as Menkes, Wilson [19], Alzheimer's, and prion diseases [20].

Aluminum holds the position of the most abundant metal by weight in the earth's crustand is nearly 8% of the total minerals. Various types of pharmaceuticals such as antacids, and cooking utensils contain aluminum [21]. Al^{3+} ions are lethal to plants and kill fish in water contaminated with acids [22] they have also been implicated in Alzheimer's and Parkinson's diseases [23]. Therefore selective and sensitive detection of Al^{3+} ions is urgently required. However, its poor coordination capability, strong hydration aptitude and lack of spectroscopic characteristics have restricted the development of analytical methods. Al^{3+} ions prefer a coordination sphere of N and O as coordinating sites [24]. In this context it is important to note that rhodamine-Al^{3+} ensembles have been reported as a chemosensor for pyrophosphate ($P_2O_7^{4-}$) using a metal displacement approach [25]. In this approach, $P_2O_7^{4-}$ has a stronger affinity for the already complexed metal resulting in metal displacement upon $P_2O_7^{4-}$ binding.Therefore, the ensemble is a chemosensor of $P_2O_7^{4-}$.

Keeping in mind the outstanding properties of rhodamine and inspired by the above reports we have engineered a novel rhodamine B salicylaldehyde hydrazone bearing an allyl group **1** (Fig. 1). Where, the allyl group behaves as both an electrophilic center, and nucleophilic center. The allylic substituent behaves like a chameleon since it changes color depending on its environment such as with the change of metal ions in the solid state. Therefore, enhancing the photophysical properties of the system and justifying its incorporation as a substituent. Probe **1** selectivelydetectsCu^{2+} and Al^{3+} ions. The **1**-Al^{3+} ensemble recognizes$P_2O_7^{4-}$ ions selectively among other tested anions. Interestingly, the fluorescence from **1**-Al^{3+} is quenched upon binding with $P_2O_7^{4-}$ anions and its color changes from pink to colorless at the same time. Thus, **1**-Al^{3+} acts as a metallo receptor for the recognition of $P_2O_7^{4-}$ ions and enables **1** to work as an OFF-ON-OFF type sensor. The real life application of **1** for Cu^{2+} and Al^{3+} ions can be demonstrated using a TLC plate test and contaminated water samples.

Inspired by the excellent photophysical properties of **1** in solution and the response to different metal ions in the solid state, probe **1** can be used as photo luminescent materials for dye lasers [26], organic light emitting diodes (OLEDs) [27], data recording and storage [28], and security printing [29]. In contrast, multi-stimuli responsive photo luminescent materials alter their optical outputs in response to external stimuli [30]. These smart materials responded to external stimuli with reversible changes to their chemical constitution or superstructures in the solid state, causing them to produce different luminescent colors. Coding of these fluorescent colors in one or two dimensions is a practice which is similar to digital coding in computer science [31] which is a potential strategy to prevent tampering or counterfeiting. Stimuli-responsive photo luminescent materials, however, can only provide a small matrix of colors as optical codes. Developing wide-spectrum tunable photo luminescent solid materials with multiple fluorescent emissions (a large matrix) remains a major challenge.

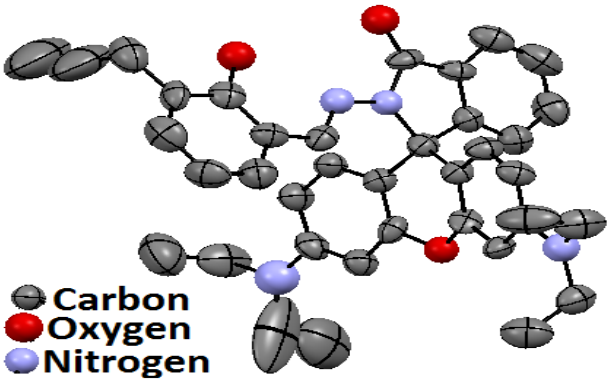

Fig.1. ORTEP (Oak Ridge Thermal-Ellipsoid Plot Program) diagram of **1** drawn at 40% probability level, hydrogen atoms are omitted for clarity.

2. Experimental

2.1. Materials

Reagents and solvents were obtained from commercial sources. Dried and distilled solvents were used in the experiments. All ^{1}H and ^{13}C NMR spectra were recorded on a JEOL AL500 FT-NMR spectrometer and chemical shifts were recorded using TMS as an internal reference.UV-Vis spectra were recorded using Shimadzu UV-1601 spectrophotometerand IR spectra were recorded on a Varian 3300 FT-IR Fluorescence was recorded on a Perkin Elmer Fluorescence spectrophotometer in H_2O:CH_3CN (3:7, v/v, HEPES buffer, pH 7.4). Electrospray ionization mass spectrometry (ESI-MS) was recorded on AMAZONSL Max ion trap mass spectrometer. Slow evaporation of **1** in ethyl acetate solution gave crystals suitable for X-ray analysis and data was collected by mounting crystal of **1** on the glass fiber of an Oxford diffraction XCALIBUR-EOS diffractometer. Monochromated Mo Kα radiation (λ = 0.71073 Å) was used for the measurements. The crystal structure of **1** was solved using the SHELXS-97 program [32] and refined using full matrix least squares (SHELXL-97) [33]. The nature of the coordination of Al^{3+} and Cu^{2+} with **1**, can be explained using energy-optimized structures at the B3LYP level with basis set 6-31G** and LANL2DZ using the Gaussian 09 program [34].

2.2. Synthesis of 1

Rhodamine hydrazone (**1**) was prepared by the reaction of rhodamine B hydrazide with 3-allyl salicylaldehyde in absolute ethanol. To an ethanolic solution of rhodamine hydrazide (0.460 g, 1.0 mmol) 3-allyl salicylaldehyde (0.273 g, 1.1 mmol) was added and

the reaction mixture was refluxed for 12 h under an inert atmosphere. On cooling to room temperature, a light pink precipitate was obtained, which was filtered and dried under *vacuo*. Yield=70%. ^{1}H NMR (500MHz, $CDCl_3$): δ 11.13 (s, 1H, -OH), 8.85 (s, 1H, -CH=N), 7.98 (t, J = 6.6 Hz, 1H, -Ar), 7.98(d, J = 6.5 Hz, 2H, -Ar),7.10 (m, ,2H, -Ar), 7.01(s, 1H, -Ar), 6.50–6.43(m, 4H, -Ar), 6.24(d, J = 7.5 Hz, 2H, -Ar), 3.31(m, 8H, $-CH_2$), 1.15(t, J=6.6Hz, 12H); ^{13}C NMR (125 MHz, $CDCl_3$): δ 164.32, 156.44, 153.35, 151.83, 149.14, 131.46, 129.72, 128.15, 128.46, 127.53, 124.07, 123.45, 118.53, 115.54, 108.28, 105.24, 98.04, 66.06, 44.45, 33.76, 12.67; IR (KBr, cm^{-1}): ν = 3432, 2971, 1714, 1693, 1634, 1615, 1516, 1467, 1308, 1265, 1219, 1119, 1078, 821, 756; Elemental analysis (calcd. %) for $C_{38}H_{40}N_4O_3$: C, 75.97; H, 6.71; N, 9.33; Found: C, 75.60; H, , 6.24; N, 9.10.HRMS (ESI-TOF) m/z $[M+1]^+$Calcd. for $C_{38}H_{40}N_4O_3$ 601.3002, found 601.3119.

2.3. Detection of $Cu^{2+}$and Al^{3+} ions in real samples

For real sample analysis three water samples (river, pond and lake) were prepared. Initially **1**(10 μM) was added to all water samples (3.0 mL) followed by the addition of different concentrations (0–10 μM) of $Cu^{2+}$and Al^{3+} ions independently.

2.4. Live cell imaging studies in SiHa Cells

SiHa, a cervical cancer cell line acquired from National Centre for Cell Science (NCCS), Pune, India were maintained and cultured in DMEM (Delbeco Modified Eagle's Medium) supplemented with 10% Fetal Bovine Serum (FBS). Cells were grown on cover slips placed in a 12 wells culture plate inside a CO_2 incubator containing 5% CO_2 at 37ºC. For the experiment of live cell imaging, the fully grown cells were washed twice with 1X PBS (pH 7.4) for 5 minutes each. After that, cells were incubated independently with 10μM **1** and 100μM $Al(NO_3)_3$ for 40 min at room temperature. For *in vivo* detection of Al^{3+} ions, firstly the cells were treated with 10μM of **1** for 25 min followed by addition of 100μM $Al(NO_3)_3$ and incubated for 15 min. In separate wells, cells were also incubated with 200μM pyrophosphate (for 40 min), $Al(NO_3)_3$ (40 min) and both together (25 min) with **1**(15 min). In parallel, cells were treated with 100 μM $Cu(NO_3)_2.3H_2O$ alone in a separate well for 40 min at room temperature. Further, in separate wells, cells initially treated with 10 μM of **1** for 25 min 100 μM $Cu(NO_3)_2.3H_2O$ was added for 15 min. After the incubation, the cells were washed two times with 1XPBS to remove

unbounded compounds and cell nuclei were counter stained with DAPI (1µg /ml). After a brief wash the cells were mounted with 1XPBS on glass slides. The fluorescence images were captured using a Nikon NiU-Upright fluorescence microscope.

3. Result and discussion

A new rhodamine hydrazone **1** has been prepared in good yield (86%) by the coupling of 3-allyl salicyaldehyde with rhodamine hydrazide in absolute ethanol as depicted in Scheme 1.

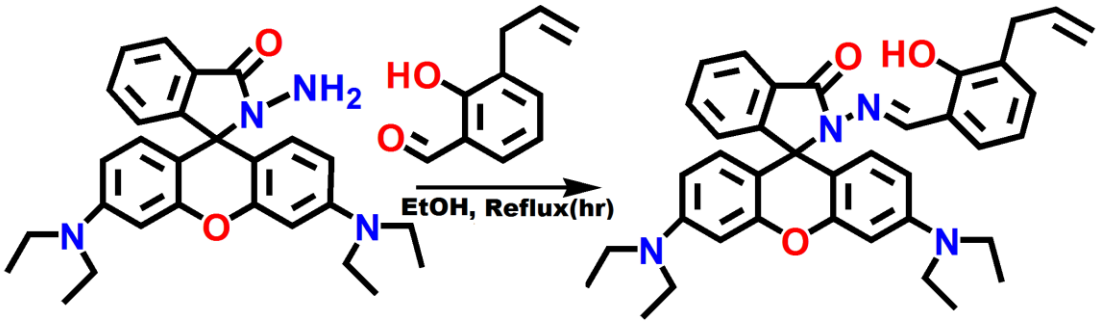

Scheme 1: Synthesis of **1**

Probe **1** was fully characterized using numerous physico-chemical techniques (Fig.S1–S3, ESI). Probe **1** crystallizes in the monoclinic crystal system with P21/n space group and its structural parameters, selected bond distances (Å) and bond angles (deg) are given in the ESI Table S1 and Table S2 whereas the selected parameters for weaker interactions are listed as ESI Table-S3. Probe **1** shows a dihedral angle of 89.40º between xanthene and aldehydic containing components (Fig. 2a). It also forms one classical and one non classical intra-molecular hydrogen bond between O002-H002----N2 with a distance of 1.87 Å and C034-H03D----O002 with a distance 2.40 Å, respectively as depicted in Fig. 2b. The molecules display a ladder structure (Fig. 2c) associated *via* non classical intermolecular H-bonds between the C030--H03A group of the diethyl amino part of one molecule and O004 of the carbonyl group of another molecule of probe **1**. Probe **1** also shows C-H···π interactions explicitly represented as C039-H03N···π are listed in ESI Table S4, satisfying four parameters (C···πm≤4.3Å, H···πm≤3.8Å, C-H···πm≥120°, C-πm-πn≤30°) [35] which is mandatory for non-canonical interactions. The C-H···π interaction results in a helical structure as depicted in Fig. 2d Aromatic stacking interactions between the aldehydic benzene ring of two molecules of probe **1** with interplanar separation of 3.761 Å, leads to the formation of a series of crosses, arranged in parallel (Fig. 2e).

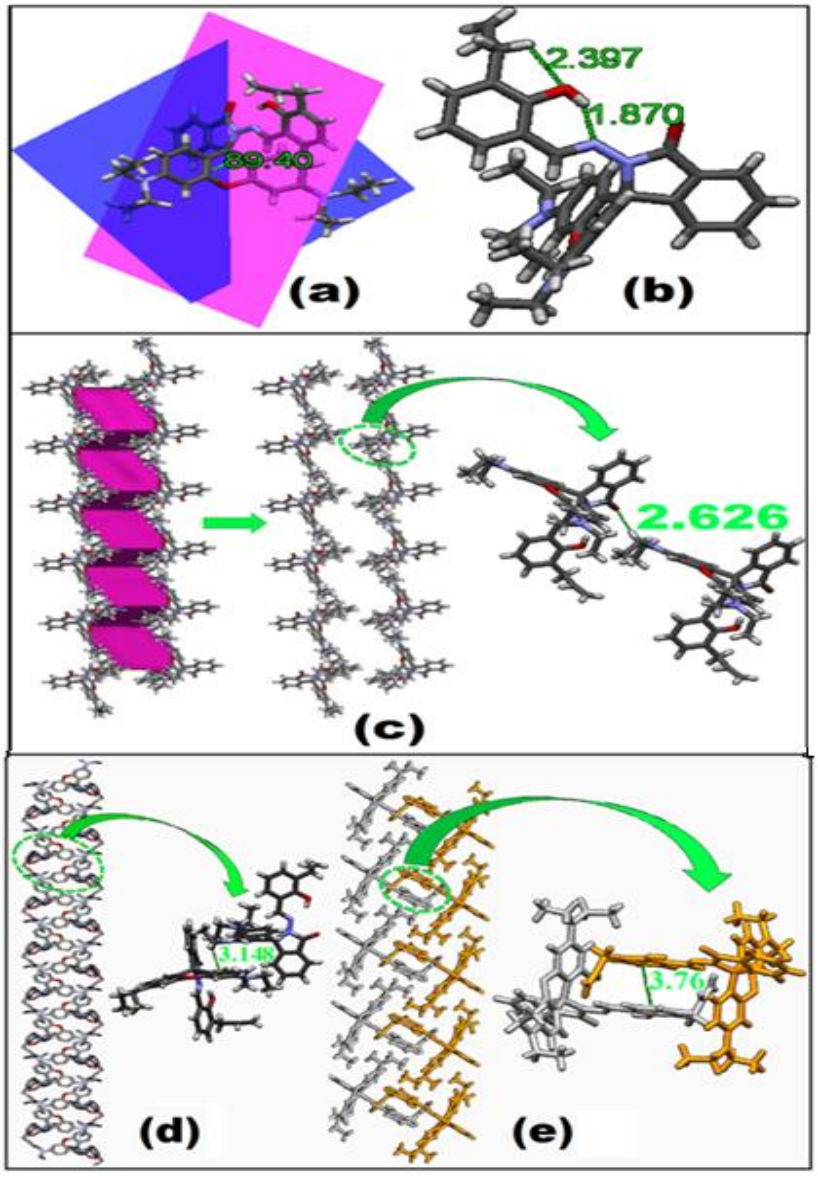

Fig.2. (a) Dihedral angle between two coordination planes, (b) classical and non classical intramolecular H-bond, (c) formation of ladders *via* non classical intermolecular H-bonding, (d) C-H···π interactions producing helical chains and (e) π-π stacking interactions producing crosses**.**

3.1. Spectroscopic recognition of Cu^{2+} and Al^{3+} ions:

To investigate the spectral response of **1**, in H_2O: CH_3CN (3:7, v/v, HEPES buffer, pH 7.4) UV-visible and fluorescence titration experiments were carried out using common and competitive analytes. The UV–vis spectrum of **1** (10.0 μM) displayed peaks centered at

λ_{max}=239nm (ε=62,000 $M^{-1}cm^{-1}$), λ_{max}=276nm (ε=40,300 $M^{-1}cm^{-1}$) and at λ_{max}=308nm (ε=28,500 $M^{-1}cm^{-1}$) all the three bands are ascribe to π-π transitions. (Fig. S4 ESI) In order to investigate the interaction of **1** with metal ions, a solution of **1** was treated with different cations *viz.*, Li^{+}, Na^{+}, Ca^{2+}, Fe^{3+}, Al^{3+}, Sn^{4+}, Mn^{2+}, Co^{2+}, Ni^{2+}, Cu^{2+}, Zn^{2+}, Cd^{2+}, and Hg^{2+} (as nitrate salts; 10.0 equiv.) and it was observed that the absorption spectrum of **1** only changes with Cu^{2+} and Al^{3+} ions while the other metal ions investigated resulted in negligible changes (Fig. S5 ESI).

The addition of Cu^{2+} and Al^{3+} (10.0 equiv) ions separately to a solution of **1** caused a new band to appear at λ_{max}= 552nm and λ_{max}= 559nm respectively. The absence of this significant peak in free receptor **1** indicates that the spirolactam bond remains intact *i.e.* in its closed form. Upon addition of Cu^{2+} and Al^{3+} ions the color of **1** change from colorless to pink clearly observed using the naked eye (Fig. S6 ESI) which indicates the breaking of the spirolactum bond and delocalization of the xanthene part of the rhodamine group. This observation was supported by the peaks observedin the visible region of the spectrum. Spectrophotometric titrations were performed in order to understand the interaction of **1** (H_2O:CH_3CN (3:7, v/v, HEPES buffer, pH 7.4) with aqueous solutions of Cu^{2+} and Al^{3+} (1.2 equiv. each) at 25°C. "Turn on" responses were obtained for 1-Cu^{2+} (Fig. 3a) and 1-Al^{3+} (Fig. 3b). Thus the addition followed excellent linear relationship with increasing Cu^{2+} and Al^{3+} concentrations after that a plateau was reached, at 1.2 equiv. indicating that saturation had occurred for both Cu^{2+} and Al^{3+} ions (inset of Fig.3a and 3b respectively).

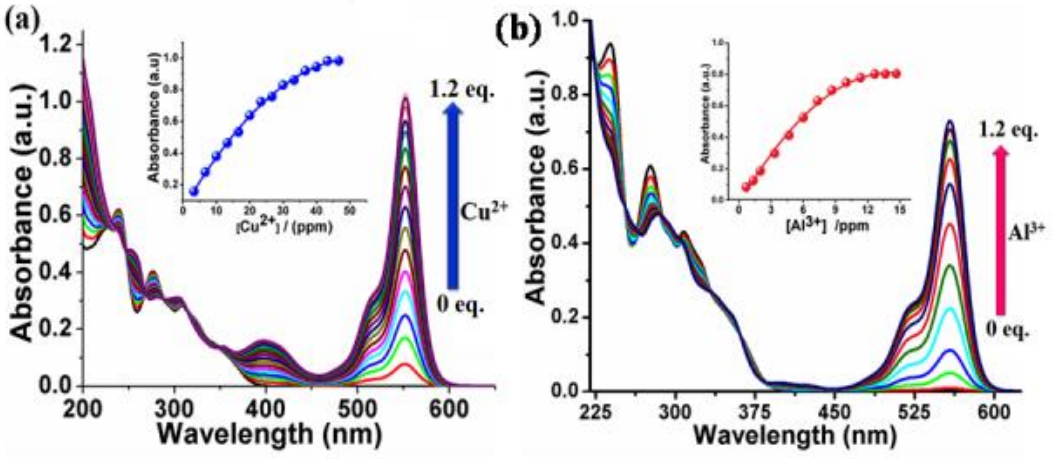

Fig. 3. Changes in the absorbance of **1** (1.0×10^{-5} M, H_2O:CH_3CN, 3:7, v/v, HEPES buffer, pH 7.4) on the addition of 0–1.2 equiv. of (a) Cu^{2+} and (b) Al^{3+}in H_2O (insets display variation of

absorbance at λ_{max} = 552nm as a function of ppm concentrations of Cu^{2+} and at λ_{max} = 559nm for Al^{3+} ions respectively).

To investigate the molecular interactions between **1** and cations fluorescence spectroscopy is an important tool because of its high sensitivity. The sensing availability of **1** with various metal ions was examined, by recording the fluorescence spectra of **1** after the addition of representative analytes in H_2O:CH_3CN (3:7, v/v, HEPES buffer, pH 7.4). Except Al^{3+} ions the addition of metal ions exhibited negligible fluorescence enhancements (Fig.4a). Probe **1** is non-fluorescent due to the stable spirolactam form, and among the metal ions added only Al^{3+} ions were able to show "Turn-On" fluorescence response with a band at λ_{max}=587 nm. As the amount of Al^{3+} increased, the fluorescence intensity gradually increased attaining a constant value at 1.2 equiv. (Fig. 4b). The enhancement in fluorescence intensity for Al^{3+} ions may be attributed to chelation enhanced fluorescence (CHEF) in addition to the normal ring opening. The addition of Al^{3+} ions followed a sigmoidal pattern (inset of Fig.4b).The fluorescence quantum yield of **1** using quinine sulphate as standard was found to be φ=0.029 the addition of Al^{3+} ions enhanced the value 10.1 times (φ=0.303). The fluorescence of the spirolactam ring-opened form of rhodamine was quenched by Cu^{2+} ions because of chelation enhanced fluorescence quenching (CHEQ).

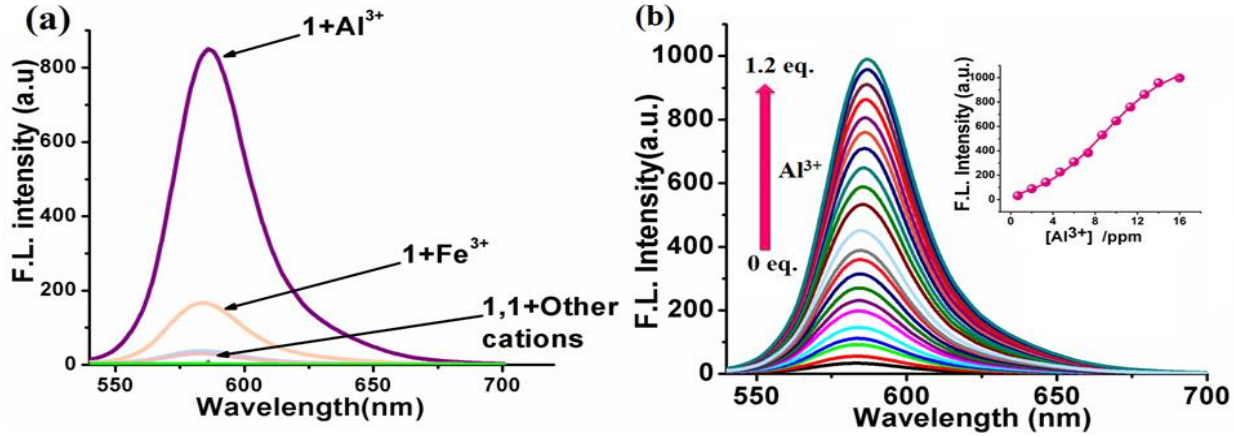

Fig. 4. Emission intensity changes of **1**($1x10^{-5}$M) upon addition of (a) cations (Li^+, Na^+, Ca^{2+}, Fe^{3+}, Al^{3+}, Sn^{4+}, Mn^{2+}, Co^{2+}, Ni^{2+}, Cu^{2+}, Zn^{2+}, Cd^{2+}, and Hg^{2+} ions) (10 eq.) in H_2O:CH_3CN (3:7, v/v, HEPES buffer, pH 7.4) and (b) various concentrations of Al^{3+}. Inset shows the variation of fluorescence intensity with Al^{3+} ion concentration.

The stoichiometry of the **1** and the metal ions (Cu^{2+} and Al^{3+}) was established using a Job's plot analysis.The total concentration of **1** and metal ions was kept constant at 10 μM while the mole fraction of Cu^{2+} and Al^{3+} ions was varied from 0.1 to 0.9 (Fig. S7a and S7 b ESI) In both cases, the curve maximum corresponded to a 0.5 mole fraction, indicating a 1:1 complex between **1** and Cu^{2+} and Al^{3+} ions. For both Cu^{2+} and Al^{3+} ions, the calibration plot is linear (Fig. S8a and b ESI) and the detection limit of **1** for Cu^{2+} and Al^{3+} was 321 nM and 572 nM respectively [36]. The binding constants calculated (Fig. S9a and b ESI) using the Benesi–Hildebrand method [37] for Cu^{2+} and Al^{3+} ions were $6.2\times 10^4\ M^{-1}$ and $1.4\times 10^4\ M^{-1}$ respectively using the UV-visible data for Cu^{2+}ions and fluorescence data for the Al^{3+} ions.

3.2. Interference studies

Selectivity is one of the essential features for a probe responding to metal ions. Therefore, interference towards different metal cations was also evaluated (Fig. S10a ESI) The results indicate that the coexistent metal cations, including Li^{+}, Na^{+}, Ca^{2+}, Fe^{3+}, Sn^{4+}, Mn^{2+}, Co^{2+}, Ni^{2+}, Zn^{2+}, Cd^{2+} and Hg^{2+} barely affect the recognition of Cu^{2+} and Al^{3+} ions. Notably, Cu^{2+} was found to be the predominant input in the case where Cu^{2+} and Al^{3+} ions were taken together. Probe **1** exhibits greater selectivity for Cu^{2+} in UV-visible analysis. Similarly, negligible change in the fluorescence intensity was observed for **1** (10 μM) with Al^{3+} (1 equiv.) in the presence of the tested cations (1.0 equiv., except the Cu^{2+} ion), as depicted in Fig.S10b ESI. The distinctive selectivity of **1** for Cu^{2+} and Al^{3+} ions may be attributed to the coordination geometry and conformation of the receptor and the size of the cations.

3.3. NMR titration

In order to strengthen our mechanism and plausible binding mode ^1H NMR titrations were performed. As shown in Fig. S11, ESI peaks for protons corresponding to the imine and xanthene are deshielded on addition of 1.0 equiv. of Al^{3+} ions and the N=CH proton moves downfield from δ=8.82 ppm to δ=9.47ppm which indicates that Al^{3+} ions bind to the "N", thereby lowering the electronic density ofthe imines hydrogen. In addition the downfield shift of the OH proton occurs and finally it disappears, supporting deprotonation of **1**. The downfield shift of the aromatic peaks occurs due to the delocalization on the xanthene moiety. The above results indicate that a plausible binding mode of **1**-Al^{3+} includes a coordinated "N", spirocarbonyl "O" and OH.

3.4. Reversibility

Reversibility is among one of the options which need to be ticked for a receptor to fall into the category of an ideal receptor. The reversible binding of **1** to Cu^{2+} and Al^{3+} ions was investigated through absorption and fluorescence titrations by the addition of various anions. Only $EDTA^{2-}$(1.0 equiv. aqueous solution of $EDTA^{2-}$) and $P_2O_7^{4-}$(1.0 equiv. aqueous solution of $P_2O_7^{4}$) bleaches the "signal-on" absorption bands for Cu^{2+} ions and emission band for Al^{3+} respectively. It could be understood that $EDTA^{2-}$ demetallates the Cu^{2+}ions from **1**-Cu^{2+} solutions. This process regenerates the spirolactam ring of **1** supported by the reappearance of its original color. Probe **1** displayed good reversibility for at least five cycles (Fig. 5a and 5b).While reversibility in case of Al^{3+} ions can be displayed with $P_2O_7^{4-}$ ions. Under a UV lamp beautiful orange fluorescence was observed for **1**-Al^{3+} but on addition of $P_2O_7^{4-}$ ions the initial fluorescence was restored the reversible nature was further corroborated by the fluorescence reversibility experiment as depicted in Fig 5c and 5d.

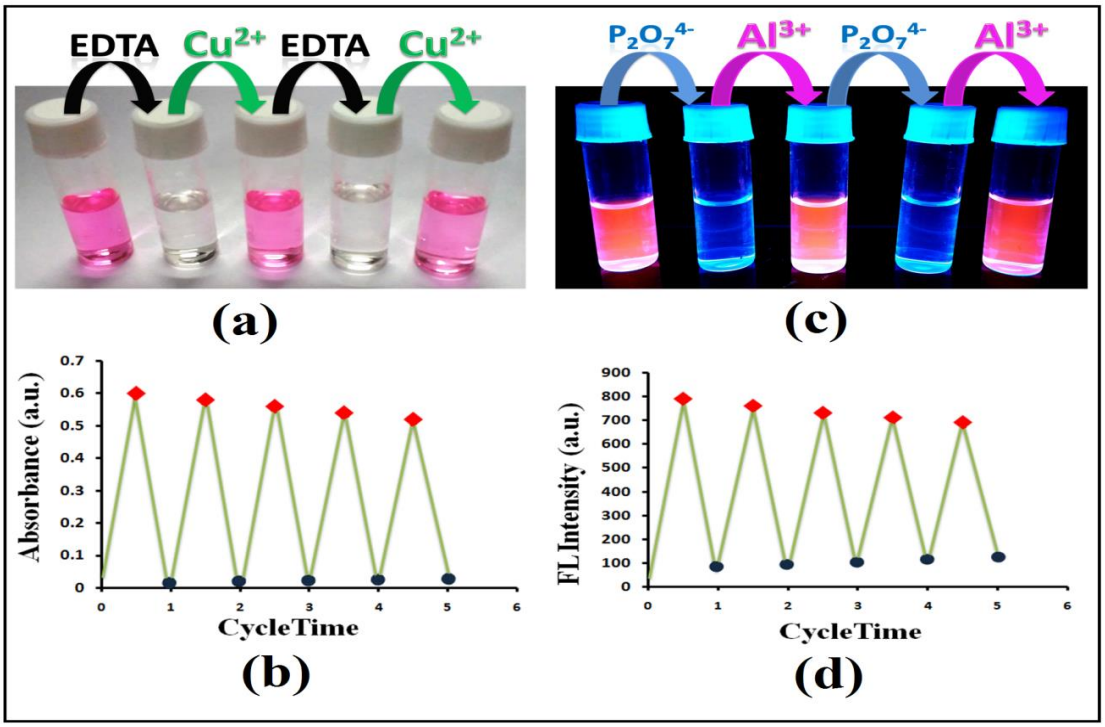

Fig. 5. Reversible cycle of **1** with Cu^{2+} and $EDTA^{2-}$ by (a) naked eye and (b) absorbance changes; Reversible cycle of **1** with Al^{3+} and $P_2O_7^{4-}$ by (c) naked eye under UV lamp and (d) emission intensity changes.

3.5. pH study

To optimize the suitable experimental pH value, the variation of the fluorescence intensity from probe **1** in the absence and presence of Al^{3+} ions has been investigated. As depicted in Fig. S12a, ESI), the fluorescence intensity from **1** recorded at λ_{em} 587 nm increases with the decrease of the pH value. It owes to open-ring structure of the rhodamine. However, above pH > 6.0, the fluorescence intensity from **1** remains almost constant owing to the closed spirolactam ring of the rhodamine. The fluorescence intensity from **1**+Al^{3+}, was also found almost constant between pH 6.0 and 8.0, which might be ascribed to the chelation enhanced fluorescence and ring opening of the rhodamine with Al^{3+}. The variation of the absorbance of **1** and **1**-Cu^{2+} was also found consistent with the similar pH range (Fig. S12b, ESI). Thus, in view of these observations and also in view of the physiological pH value of 7.4, all experiments have been performed at pH 7.4.

3.6. TLC plate test

TLC plates coated with probe **1** have been prepared for the detection of Cu^{2+} and Al^{3+}ions in water (Fig. S13, ESI). Other tested metals were unable to show any color change in their respective solution as well as on TLC plates.

3.7. Plausible mechanism

In order to validate our proposed reaction mechanism (Scheme 2) of **1** with Cu^{2+} and Al^{3+} ions, the ESI–MS analysis (Fig. S14a and b, ESI) was utilized. A peak at m/z 724.66 corresponding to [Cu(**1**)(NO_3)] was observed upon the addition of Cu^{2+} to a CH_3CN solution of **1** and a peak a at m/z 768.40 corresponding to $[M-1]^+$ where M=[Al(**1**)(NO_3)$_2$(H_2O)] was observed upon the addition of Al^{3+} to an acetonitrile solution of **1**. To further strengthen the explanation, the IR spectra of **1** and **1**-Cu^{2+} are given in Fig. S15a and b, ESI The amide carbonyl (C=O) vibrations observed at 1714 cm^{-1} shifted to 1704 cm^{-1} and 1707 cm^{-1} for Cu^{2+} and Al^{3+} ions respectively. Indicating that the amide spiro-carbonyl O atom(CO) of the rhodamine B group coordinates with both of the relevant ions. The ν (C=N) vibration shifted from 1615 cm^{-1} to 1589 cm^{-1}. A peak observed at 1384 cm^{-1} was attributed to ν(N-O) vibration of the NO_3^- group for both Cu^{2+} and Al^{3+} ions.

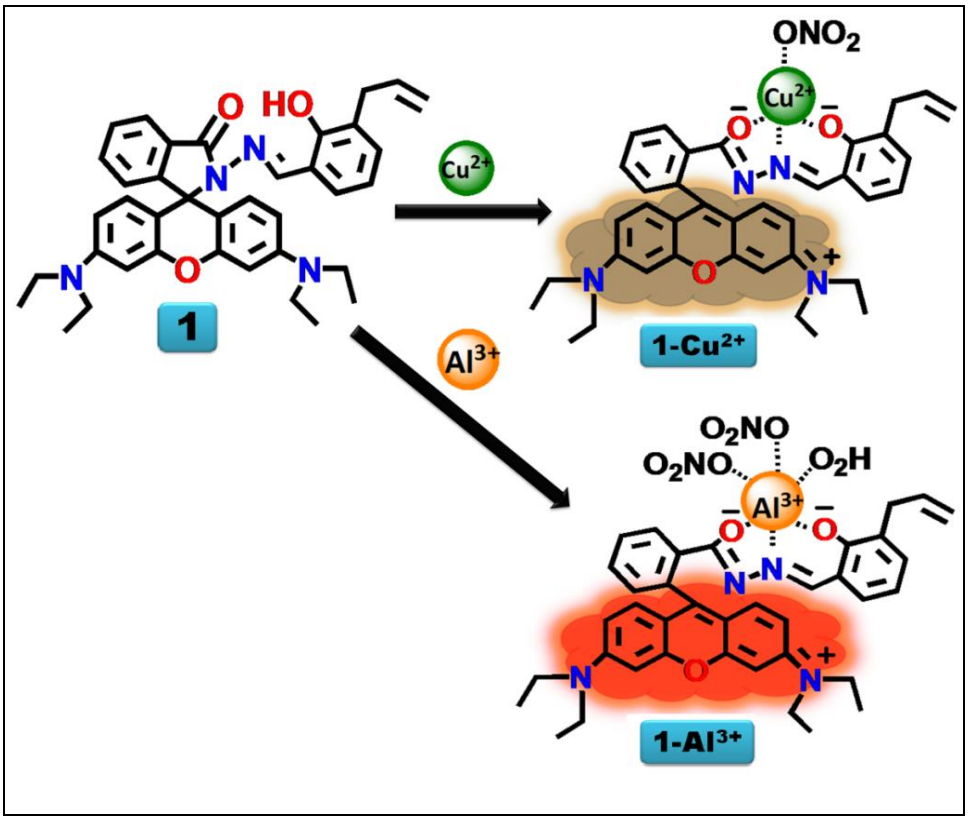

Scheme2. Plausible binding mode of probe **1** separately with Cu^{2+} and Al^{3+}

3.8. Fluorescence sensing of 1-Al^{3+} ensemble towards $P_2O_7^{4-}$

The reversibility of probe **1** using $P_2O_7^{4-}$ added to a solution of the **1**-Al^{3+}ensemble has been shown above. **1** Alone cannot detect the presence of pyrophosphate anion as shown in ESI Fig. S16, ESI. Therefore, the ensemble (**1**-Al^{3+}) was allowed to interact with other anions (F^-, CN^-, NO^{3-}, $P_2O_7^{4-}$, H_2PO^{4-}, HPO_4^{2-}, AMP, ADP and GMP) (Fig. S17, ESI). But, only $P_2O_7^{4-}$ ions were able to perturb the fluorescence spectra of the (**1**-Al^{3+}) ensemble. The fluorescence of the ensemble (1 - Al^{3+}) was quenched completely on the addition of $P_2O_7^{4-}$ions. The LOD value for $P_2O_7^{4-}$ ions was found to be $8.7x10^{-7}$M. Moreover the addition followed exponential decay as shown in the inset of Fig.6. The strong binding of Al^{3+} ions with $P_2O_7^{4-}$ leads to the dissociation of Al^{3+} ions from the **1**-Al^{3+}ensemble upon the addition of $P_2O_7^{4-}$, with revival of starting receptor **1** established by ESI–MS (Fig. S18, ESI). From the above observations a plausible mechanism for the sequential detection of Al^{3+} ions and $P_2O_7^{4-}$ ions (**1**-Al^{3+}) by **1** is shown in

Scheme 3. As shown in Fig. 6, the fluorescence of the **1**-Al^{3+}ensemble (1×10^{-5} M) at λ_{max} 587 nm decreased gradually and reached a plateau when 5.0 equiv. of $P_2O_7^{4-}$ was added.

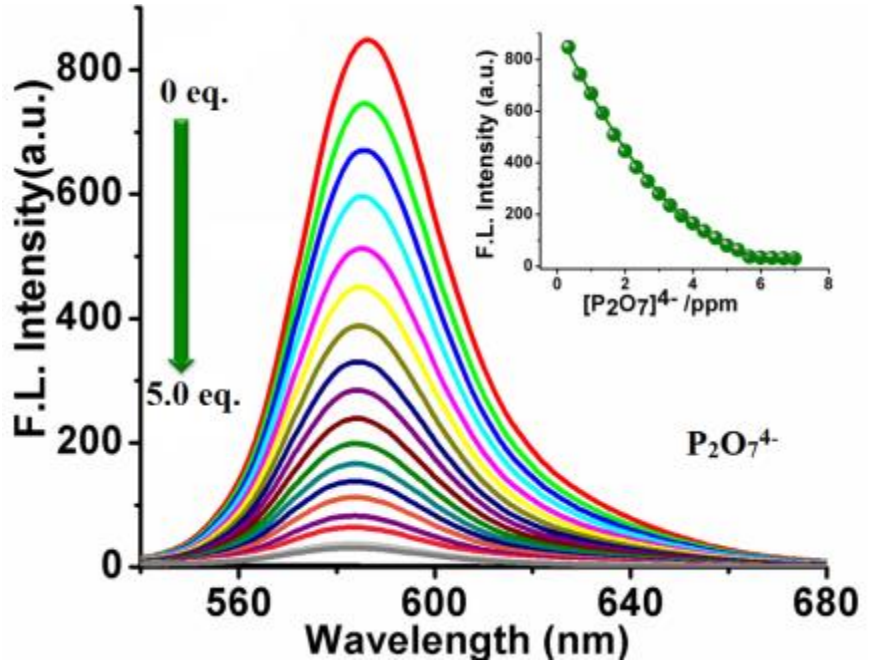

Fig. 6. Fluorescence spectra of **1**-Al^{3+} ensemble ($1x10^{-5}$ M) on the addition of $P_2O_7^{4-}$ up to 5 eq. H_2O:CH_3CN (3:7, v/v, HEPES buffer, pH 7.4); λ_{ex}= 500 nm.

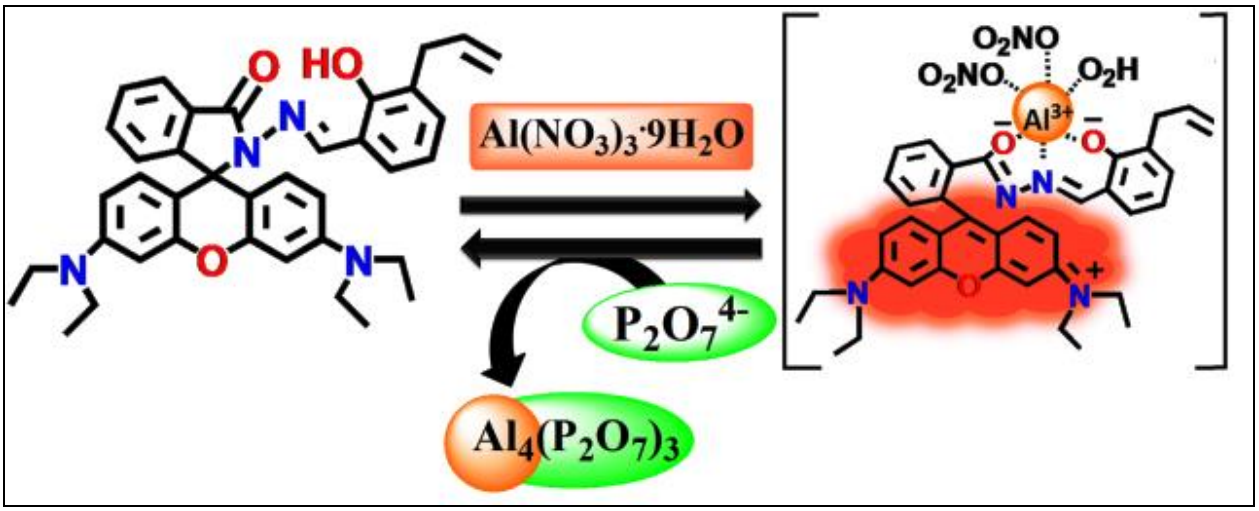

Scheme3. Possible mechanism of secondary sensing of $P_2O_7^{4-}$ ions by the **1**-Al^{3+}ensemble

3.9. Logic gate interpretation

Motivated by the fast and multiple-readouts of probe **1** towards Cu^{2+}, Al^{3+}, EDTA and $P_2O_7^{4-}$ over a large optical range (λ = 200–700 nm)(*vide supra*), sequential logic circuits and combinatorial logic circuits have been assembled. An "OFF-ON-OFF" system for probe **1** using inputs Cu^{2+} and EDTA, results in a logic circuit where Cu^{2+} works as the first input and EDTA works as second input (sequence 1). The signal change at λ_{max} =552 nm is OUT1 and the "by-eye" color change is OUT2. The threshold values have been fixed at 0.59 for OUT1 (Fig. S19 ESI) and color change from colorless to red is designated as "0" and "1"respectively (Fig. 7). When input signal is "1–0", the absorbance arises at OUT1 and the color changes tored at OUT2 ("1–1"). Continuous addition of EDTA ("1–1") recovers the initial absorbance and color (colorless) (Fig. 7). The "OFF-ON-OFF" logic functions in a feedback loop and possesses a memory feature with "write-read-erase-read" using OUT1 and OUT2 (Fig.7). Furthermore, the "OFF-ON-OFF" switch of **1** using Al^{3+} and $P_2O_7^{4-}$ can also process information in the form of two input and two output sequential logic circuits with "write-read-erase-read" functions (Fig. 8). The threshold values are fixed at 0.29 for OUT1 (Fig. S20, ESI).

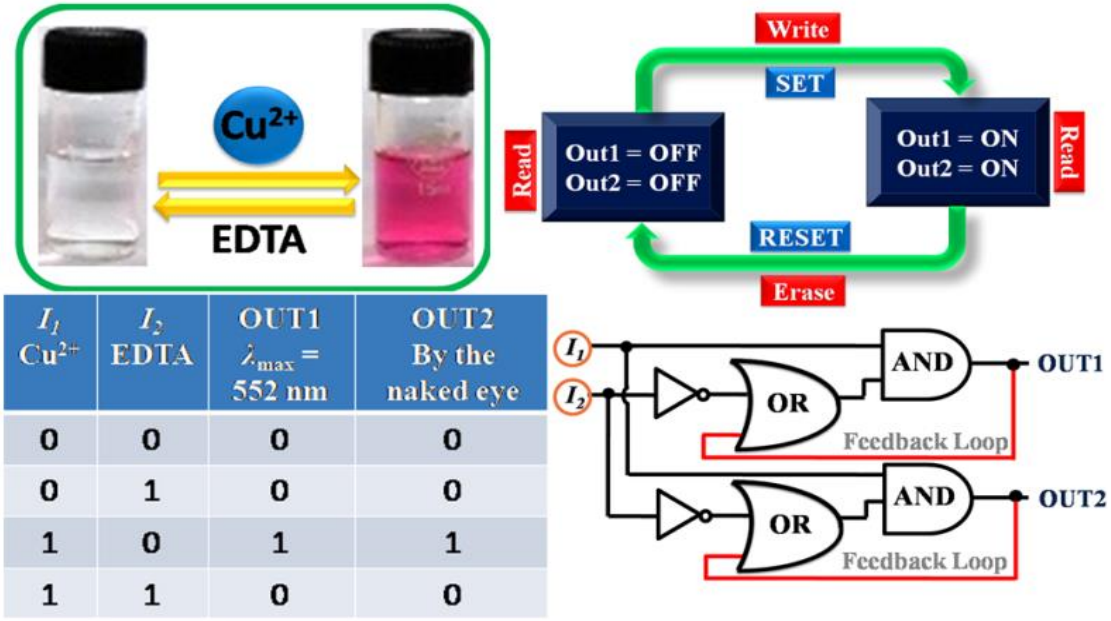

I_1 Cu^{2+}	I_2 EDTA	OUT1 λ_{max} = 552 nm	OUT2 By the naked eye
0	0	0	0
0	1	0	0
1	0	1	1
1	1	0	0

Fig. 7. Logic circuits presenting memory units with two inputs (I_1, $Cu^{2+}$and I_2, EDTA) and two outputs and demonstration of the "write-read-erase-read" functions.

Assuming Al^{3+} (I_1), $P_2O_7^{4-}$ (I_2) and Cu^{2+} (I_3) as the three inputs and monitoring the outputs at λ_{max} = 587 nm (OUT1) and "by-eye" color change (OUT2) (threshold value =300, a.u.)(Fig. S21, ESI) offer a proficient molecular system for the special handling of three different chemical inputs. The change in color from colorless to red or pink is designated as "0" and "1" respectively. Significantly, **1** displays a combinatorial logic circuit (Fig. S22, ESI).The three-input and two output example based on fluorescence modulation is very rare for this type of combinatorial logic circuit.

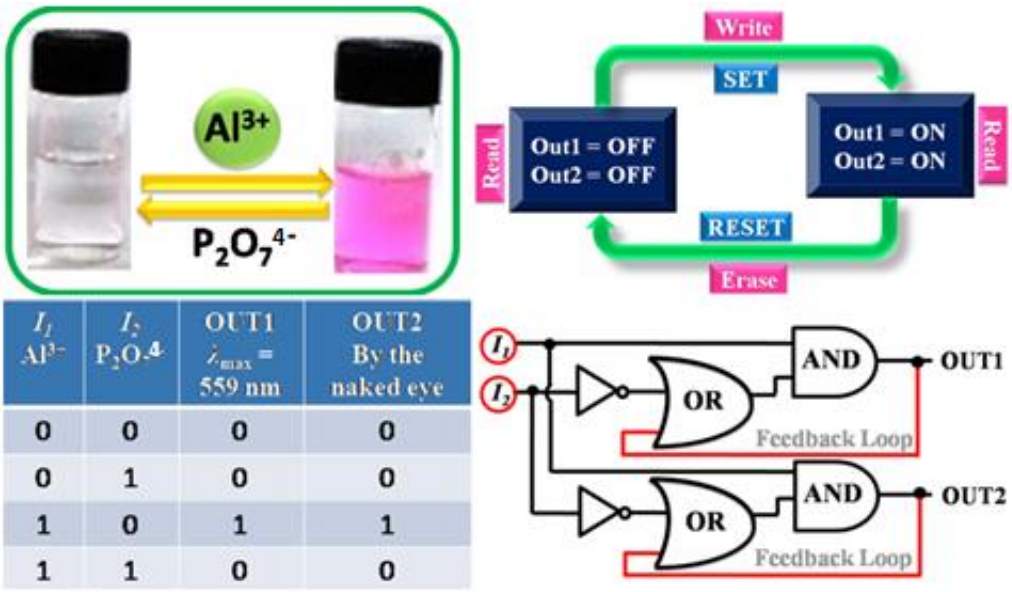

I_1 Al^{3+}	I_2 $P_2O_7^{4-}$	OUT1 λ_{max} = 559 nm	OUT2 By the naked eye
0	0	0	0
0	1	0	0
1	0	1	1
1	1	0	0

Fig. 8. Truth table, sequential logic circuits displaying memory units with two inputs (I_1, $Al^{3+}$and I_2, $P_2O_7^{4}$) and two outputs and schematic representation of the reversible logic operations for memory element holding "write-read-erase-read" functions.

3.10. SiHa cell imaging studies

Owing to the remarkable selectivity and excellent photophysical properties at physiological pH, and non-toxic character of probe **1** makes this receptor useful for the detection of Al^{3+} ions in SiHa cancerous cells. Cells incubated with **1** alone exhibited no fluorescence, whereas a red fluorescence signal was observed in cells treated with both **1** and Al^{3+} ions supporting the fluorescence turn-on behavior of **1** in the presence of Al^{3+} ions in solution (Fig.9D–D3). Moreover, red fluorescence was quenched by the addition of the pyrophosphate anion (200 μM)

(Fig. 9F–F3). Pretreated SiHa cells incubated with Cu^{2+} ions displayed weak fluorescence intensity (9H-H3). The results indicate that **1** is permeable across the cell membrane and has potential to detect Al^{3+} ions and pyrophosphate ions in living cells. Therefore, probe **1** could be employed for the real time detection of Al^{3+} ions in living cells.

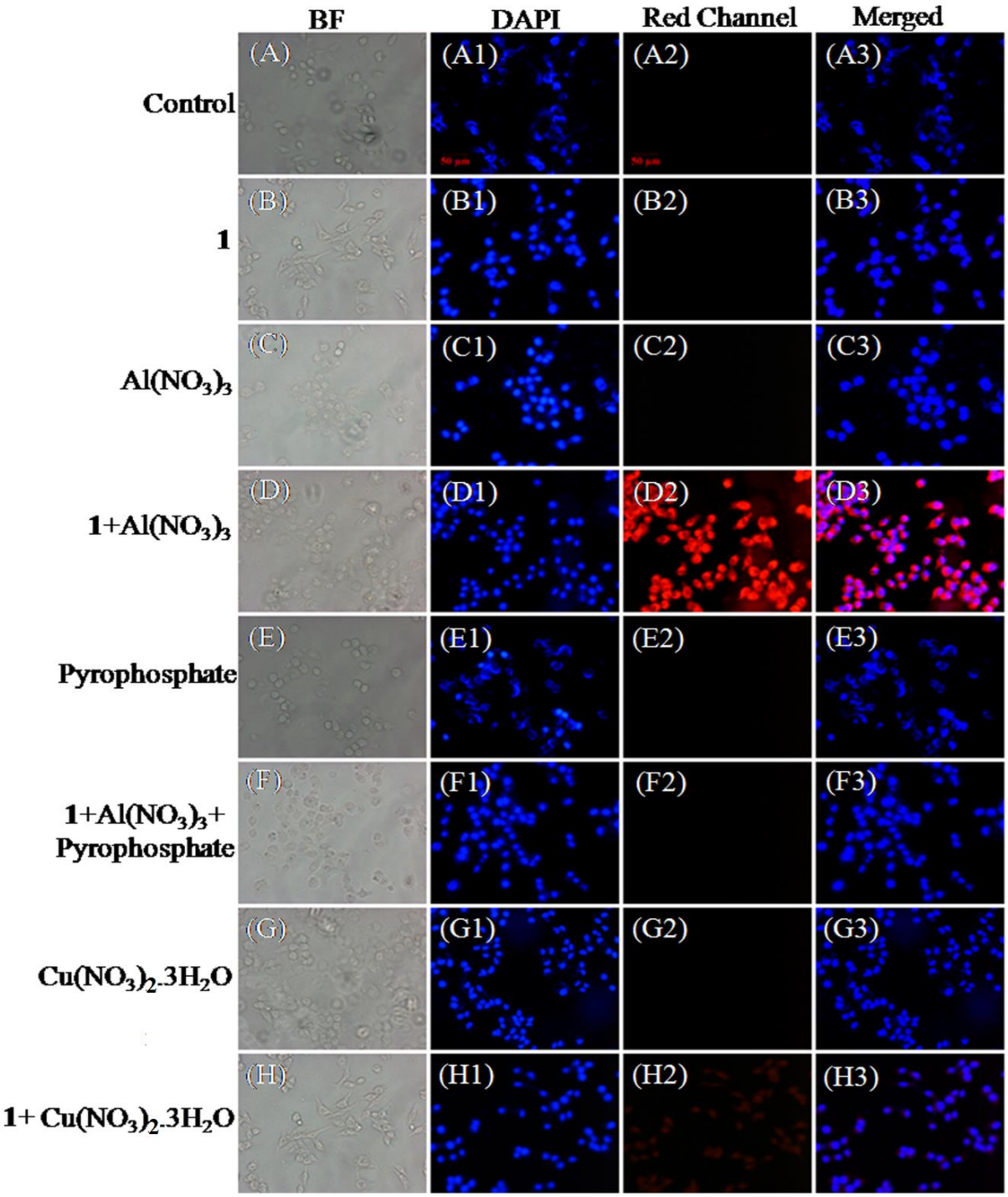

Fig. 9. Fluorescence micrographs representing OFF-ON-OFF fluorescence mechanism in the presence of **1**-$Al(NO_3)_3$-Pyrophosphate in SiHa cell. (A-H) shows bright field (BF) images at 20X, (A1-H1) shows DAPI counterstained images and (A2-H2) shows red channel [**1**+$Al(NO_3)_3$]images at 20X. Scale bar indicate 50μm. (A3-H3) are the overlaid images. The uppermost row (A-A3) represents control. The row (B-B3) shows **1**treated image, row (C-C3) only $Al(NO_3)_3$ treated images. Cells initially treated with **1** followed by treatment with $Al(NO_3)_3$displayred fluorescence (D2).Cells treated with Pyrophosphate have no fluorescence (E2), but cells initially treated with **1** followed by $Al(NO_3)_3$ when in contact with pyrophosphate show a quenched behavior (F2). The $Cu(NO_3)_2.3H_2O$ treated cells also displays no florescence (G2) but in presence of **1** weak fluorescence is observed (H2).

3.10. Theoretical studies

The energy-optimized structures of probe **1** and its metal ensembles with Cu^{2+} and Al^{3+} ions were obtained using density functional theory(DFT) calculations with the B3LYP level 6-31G** basis set for **1** and LANL2DZ basis set for metal ensembles using the Gaussian 09 program . As depicted in Fig. S23, ESI the electron density in the HOMO spreads over the entire molecule, whereas for the LUMO it is on the substituted spirolactam ring of **1**. The electron density of the HOMO orbitals in **1**–Cu^{2+} is mainly located over the xanthene moiety with little distribution on the allylic group and in **1**–Al^{3+}, theelectron density of the HOMO orbitals are principally located over the xanthene moiety. The LUMO is distributed on the allyl substituted group along with some electron density on the xanthene unit in **1**–Cu^{2+} while they are spread over xanthene moiety in **1**–Al^{3+}. The energy gaps between the HOMO and LUMO of **1**, **1**–$Cu^{2+}$and **1**–Al^{3+} were found to be 3.505eV, 2.684eV and 2.728eV respectively which indicates anenhancedstabilization of **1**-Cu^{2+} and **1**–$Al^{3+}$when compared to **1**.

TD-DFT calculations were carried out in acetonitrile medium allowing correlation of the experimentally observed electronic absorption spectra of **1** and metal ensembles with Cu^{2+} and Al^{3+}. The absorption bands calculated from TDDFT indicates three main peaks at 308, 274, and 240 nm for probe**1**. The band at λ_{max} 308 nm is dominated by HOMO−4 – LUMO and HOMO−6– LUMO transitions while the band at around λ_{max} 274 nm is dominated by HOMO−5– LUMO, HOMO−3– LUMO+1 and HOMO−1– LUMO+1transitions and the band at around 240 nm is dominated by HOMO-2 – LUMO+4, HOMO-3 – LUMO+4 transitions. For **1**–Cu^{2+} the

bandaroundλ_{max}555 nm is dominated by the HOMO–LUMO, HOMO-1 –HOMOtransitions while in **1**-$Al^{3+}$the band at around λ_{max}558 nm is dominated by the HOMO-LUMO transition. Thus the spectra calculated were found to be comparable with those obtained experimentally. The involvement of different transitions for HOMOs and LUMOs in **1**, **1**-Cu^{2+}, and **1**-Al^{3+} are depicted in Fig. 10 and the detailed UV-vis spectral data calculated for the complexes along with the assignments of different absorption bands are shown in ESI Table S5.

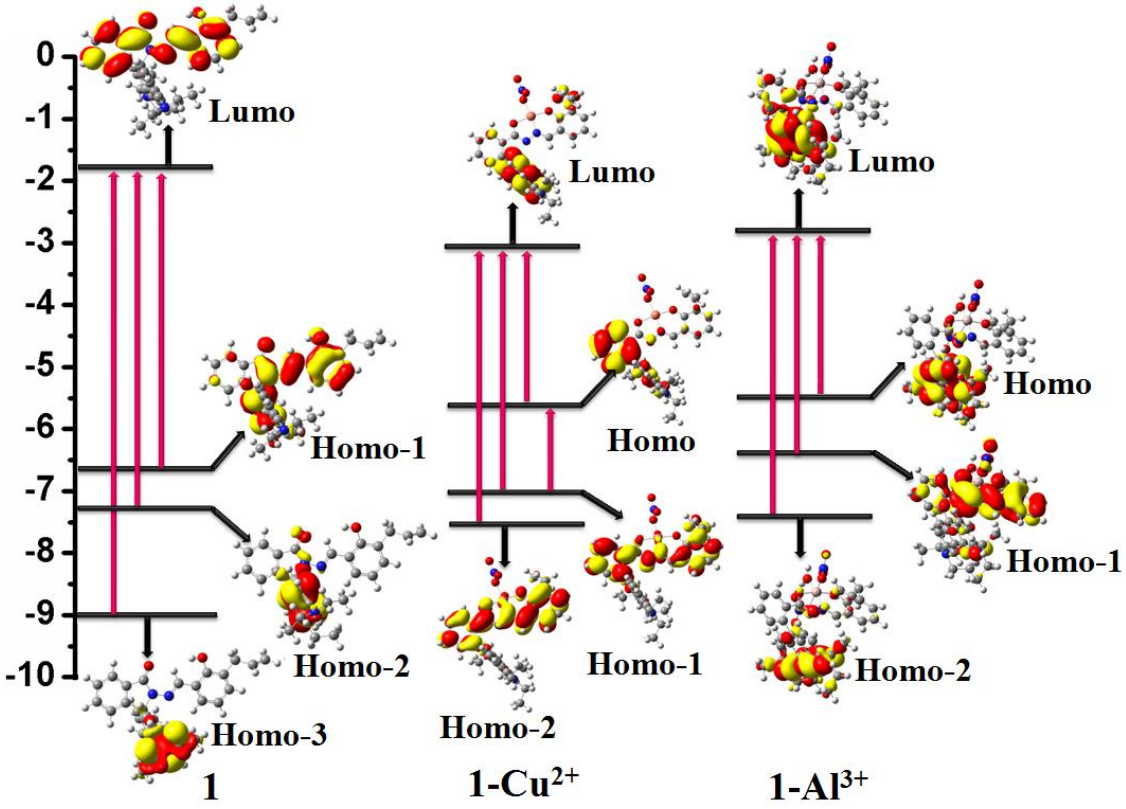

Fig.10. Energy level diagrams displaying main transitions for the lowest-energy absorption bands associated with **1**, **1**-$Cu^{2+}$and **1**-Al^{3+}in acetonitrileusing 6-31G** and LANL2DZ basis sets.

3.11. Role of **1** *for recognition of* Cu^{2+} *and* Al^{3+} *ions in water samples*

Proof-of-concept experiments were used to investigate the role of **1** in the recognition of Cu^{2+} and Al^{3+} ions in natural sources of water. Samples were collected at Varanasi City, India, from different sources such as river, pond and tap. $Cu(NO_3)_2$ solutions (0–10 μM) were spiked into these water samples followed by the addition of **1** (10 μM) a linear calibration curve between absorption and concentration was observed for

Cu^{2+} ions over a range of 3-9 μM (Fig. S24a ESI). In the same way, $Al(NO_3)_3$ solutions (0–10 μM) were spiked into water samples and **1**(10 μM) was added into these samples resulting in a linear dependence of fluorescence intensity towards Al^{3+} ions over a range from 2-11 μM (Fig. S24b, ESI). The data are given in Table S6 ESI and S7 ESI. The experimental results indicate that **1** can be used for the efficient determination of Cu^{2+} or Al^{3+} ions in ecological water sources.

3.12. Solid state properties of 1

Powder X-ray diffraction (PXRD) patterns of pristine, ground and annealed forms of probe **1** (Fig S25, ESI) were recorded. The pristine form displayed sharp peaks, which is the signature of crystallinity. Upon grinding by pestle mortar the samples displayed diffuse bands along with color changes from white to dark pink in the solid owing to the amorphous nature. However, sharp peaks appeared in the PXRD along with a change in color after annealing the ground samples at 120 °C for 15 minutes, supporting the regeneration of the crystalline form. The morphological transformation from crystalline state to the amorphous state and vice versa with color changes is connected with the mechanical switching in **1** (inset Fig. S25, ESI).

Interestingly, the presence of crystalline (I) and amorphous (II) states, could be exploited for the incorporation of a commutable binary memory state. Here two different states can be measured as writing "1" and erasing "0" of data by assuming the binary logic principle. Therefore, binary memory states could be built using, mechanical force and heat, which are capable of writing/erasing the data for processing of multi bits (''00"–''11") of information.

The pristine form of **1** displays yellow light emission at λ_{max} = 596nm (Fig. S26, ESI). On slight mechanical grinding of **1** with the salts of different metal ions (Al^{3+}, Hg^{2+}, Cd^{2+}, Co^{2+}, Zn^{2+},Ni^{2+} and Cu^{2+}), an immediate color change is observed (Fig. 11(a), Fig. S27, ESI) and red shift in emission wavelength (λ_{max} = 627 nm for **1-Al^{3+}**, λ_{max} = 639 nm for **1-Hg^{2+}**, λ_{max} = 616 nm for **1-Cd^{2+}**, λ_{max} = 625 nm for **1-Co^{2+}**, λ_{max} = 642 nm for **1-Zn^{2+}**,λ_{max} = 630 nm for **1-Ni^{2+}** and λ_{max} = 646 nm for **1-Cu^{2+}**) (Fig. 11(b)).

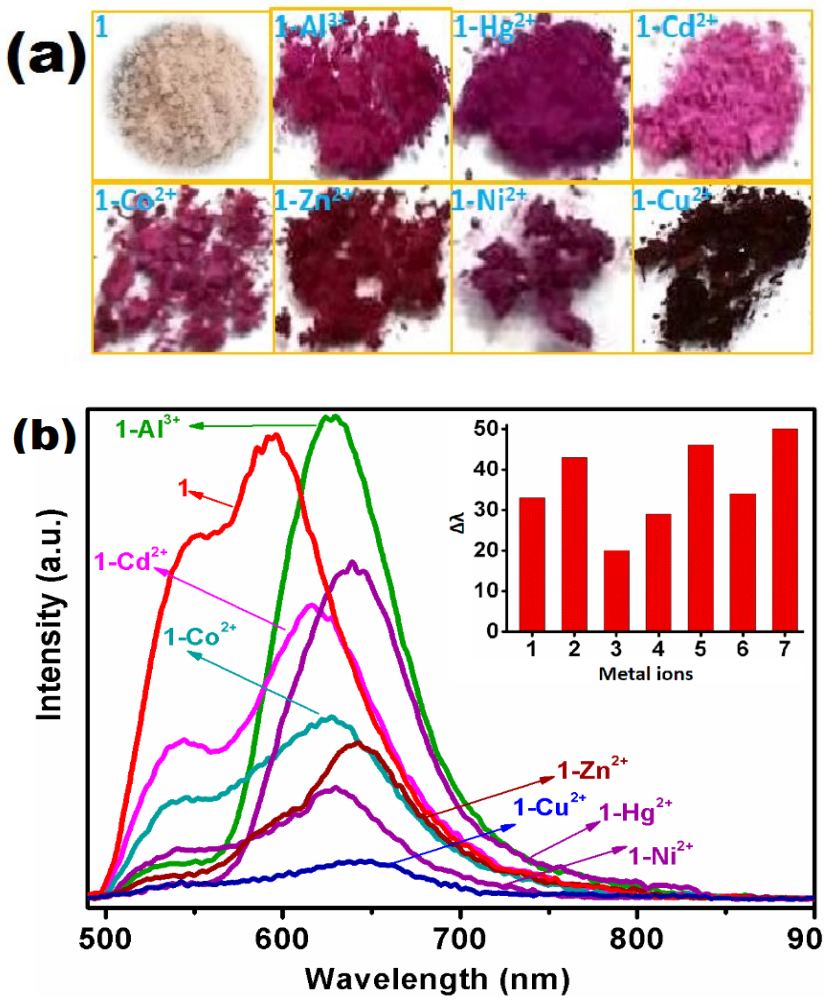

Fig.11. Visual color change upon mechanical grinding receptor **1** with the nitrate salts of different metal ions (Al^{3+}, Hg^{2+}, Cd^{2+}, Co^{2+}, Zn^{2+}, Ni^{2+} and Cu^{2+})(a) and their emission spectra (λ_{ex} = 340 nm) (b). Arrows serve as a guide to the eyes. Complete area under the peak or any wavelength in the region 500-900 nm can be utilized for "turn-on" response. Inset: Representative bar chart showing different wavelength change upon addition of various metal ions (1 = Al^{3+}, 2 = Hg^{2+}, 3 = Cd^{2+}, 4 = Co^{2+}, 5 = Zn^{2+}, 6 = Ni^{2+} and 7 = Cu^{2+}).

The major "turn-on" readout was obtained by the addition of Al^{3+} and Hg^{2+} while "turn-off" readout was obtained by the addition of Cu^{2+}. Interestingly, change in area under the peak in emission spectra or any wavelength or complete area under the peak or in the range 500-900 nm can be utilized for "turn-on" and "turn-off" response (Fig. S28, ESI). Additionally, high on/off

ratios with a fast reaction rate allows for the precise quantification of metal ions over a large optical range (λ = 500–900 nm) rather than monitoring at a single wavelength (Fig. S28, ESI). Instant color changes, different emission behavior at different wavelengths in each case confirm the remarkable sensitivity of **1** toward metal ions in the solid state. Thus, probe **1** is capable of detecting metal ions in a solid sample. The UV-Vis diffuse reflectance spectrum of **1** is shown in Fig. S29, ESI.

In the corresponding CIE diagram, 'x' and 'y' values were determines to be 0.4897 and 0.5004 for **1** in the 'orange-yellow' region of the diagram, but the color shifted towards orange-red and finally red upon addition of different metal ions (Co^{2+}, Cd^{2+},Ni^{2+}, Cu^{2+}, Zn^{2+}, Al^{3+}, Hg^{2+}) as shown in Fig.12. The largest change occurs for the addition of Al^{3+} and Hg^{2+}, the shifts occur in the red region of CIE diagram. The corresponding 'x' and 'y' values for these metal ions were (0.6275, 0.3699) for Al^{3+} and (0.6432 and 0.3535) for Hg^{2+}. The corresponding correlated color temperature (CCT) values were also evaluated in order to understand the utility of the phosphor system. The CCT value for compound **1** was determined to be 2959 K (warm color region).

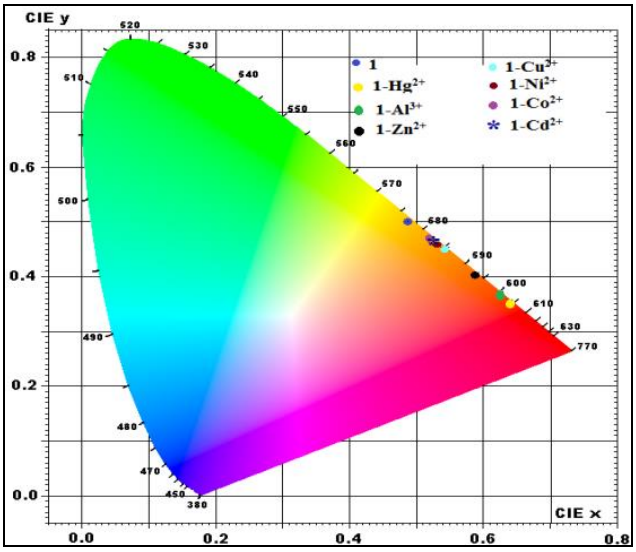

Fig. 12. CIE coordinates for **1**, **1-Al^{3+}**, **1-Hg^{2+}**, **1-Cd^{2+}**, **1-Co^{2+}**, **1-Zn^{2+}**, **1-Ni^{2+}** and **1-Cu^{2+}** in the solid state.

Upon addition of Co^{2+}, Cd^{2+}, Ni^{2+} and Cu^{2+} ions, the CCT values are 2374, 2345, 2222 and 2077 K respectively. The CIE indices and CCT values for various sample compositions are

presented in Table S8. In the chromaticity diagram a rise in the 'x' coordinate and decrease in the 'y' coordinate indicates higher color purity. The color purity was calculated the using the following formula

Color purity = $\sqrt{(x_s-x_i)^2 + (y_s-y_i)^2} / \sqrt{(x_d-x_i)^2 + (y_d-y_i)^2}$ x 100 %.

Where (x_s, y_s) are the compound coordinates, (x_d, y_d) are the dominant wavelength coordinates, and (x_i, y_i) are the illuminant pointcoordinates. In the current work, taking (x_s, y_s) = (0.4897, 0.5004) for compound **1**. (x_d, y_d) = (0.6437, 0.3535) for the dominant wavelength and (x_i, y_i) = (0.3101, 0.3162) for the illuminant point, the color purity withHg^{2+} was found to be 76.23 %. Moreover, after addition of Hg^{2+} top robe **1**, the color coordinates approaches close to the ideal red chromaticity for the National Television Standard Committee (NTSC) system. The observed high PL intensity along with brilliant color purity indicatesthat the Hg^{2+}compositeis appropriate for lighting and display uses.

Additionally, the band gaps of **1** (Fig. S30, ESI) were tuned between 2.08 eV to 1.60 eV by the addition of different metal ions (Al^{3+}, Hg^{2+}, Cd^{2+}, Co^{2+}, Zn^{2+},Ni^{2+} and Cu^{2+}). The band gaps were estimated using the Kubelka−Munk function as depicted in Fig. S30, ESI and data for different sample compositions are given in Table S8.

4. Conclusion

In conclusion, the stable duo-optical (chromogenic and fluorogenic) responses of **1** were exploited for dual optical recognition of cations (Cu^{2+} and Al^{3+}) and **1**-Al^{3+} for anion ($P_2O_7^{4-}$). The mode of interaction was established by IR, UV-visible, fluorescence, ESI-MS and ^{1}H NMR titrations studies. Moreover, **1** was found to be efficient for multiple ion detection in SiHa cells. Furthermore, stimulated by its excellent selectivity, rapid response and multiple readout two-input and two-output, three-input and two-output logic circuits have been constructed. The monitoring of the outputs *via* multiple modes (optical and visual) provides accurate quantification, widespread utility, and multi-bit information processing at different wavelengths. Notably, **1** provides label-free detection in a matrix of analytes and allows the preservation of exclusive information with no mixing. While, the visual detection of ions *via* an obvious color change in solution and ready-to- use TLC strips make probe **1** cost-effective for real world water sample analysis.

Acknowledgements

The financial assistance from UGC-BSR, India (LM), CSIR, India (AR) for senior research fellowship and Banaras Hindu University is gratefully acknowledged. AKS gratefully acknowledges the support of DST, India INSPIRE grant (DST/ INSPIRE/ 04/2015/ 002555).

Keywords: Chemosensor • Rhodamine • DFT • Real sample analysis• Photoluminescence.

Appendix A. Supplementary material

Electronic Supplementary Information (ESI) available: [CCDC reference no. 1517899] contain the supplementary crystallographic data for**1**. This data can be obtained free of charge via http://www.ccdc.cam.ac.uk/conts/retrieving.html, or from the Cambridge Crystallographic Data Centre, 12 Union Road, Cambridge CB2 1EZ, UK, fax (+44) 1223-336-033, or email: deposit@ccdc.cam.ac.uk.

References

[1] A. P. de Silva, H. Q. N. Gunaratne, T. Gunnlaugsson, A. J. M. Huxley, C. P. McCoy, J. T. Rademacher, T. E. Rice, Signaling Recognition Events with Fluorescent Sensors and Switches, Chem. Rev., 97 (1997) 1515-1566.

[2] S. Pal, N. Chatterjee, P. K. Bharadwaj, Selectively sensing first-row transition metal ions through fluorescence enhancement, RSC Adv., 4 (2014) 26585-26620.

[3] X .Chen, T. Pradhan, F. Wang, J. S. Kim, J. Yoon , Fluorescent Chemosensors Based on Spiroring-Opening of Xanthenes and Related Derivatives,Chem. Rev., 112 (2012) 1910–1956.

[4] M. Beija, C. A. M. Afonso, J.M. G. Martinho, Synthesis and applications of Rhodamine derivatives as fluorescent probes,Chem. Soc. Rev., 38 (2009) 2410–2433.

[5] Y. Yuan, S. Sun, S. Liu, X. Song, X. Peng, Highly sensitive and selective turn-on fluorescent probes for Cu^{2+} based on rhodamine B, J. Mater. Chem. B, 3 (2015) 5261-5265.

[6] R. Arumugaperumal, V. Srinivasadesikan, M.C. Lin, M. Shellaiah, T. Shuklaa, H. C. Lin, Facile rhodamine-based colorimetric sensors for sequential detections of Cu(II) ions and pyrophosphate ($P_2O_7^{4-}$) anions, RSC Adv., 6 (2016) 106631-106640.

[7] Y. Wang, H. Q. Chang, W. N. Wu, X. J. Mao, X. L. Zhao, Y. Yang, Z. Q. Xu, Z. H. Xu, L. Jia,A highly sensitive and selective colorimetric and off–on fluorescent chemosensor for Cu^{2+} based on rhodamine 6G hydrazide bearing thiosemicarbazide moiety, Journal of Photochemistry and Photobiology A: Chemistry, 335 (2017) 10–16.

[8] A. K. Mahapatra, S. Mondal, S. K. Manna, K. Maiti, R. Maji, Md. R. Uddin, S. Mandal, D. Sarkar, T. K. Mondal, D. K. Maiti, A new selective chromogenic and turn-on fluorogenic probe for copper(II) in solution and vero cells: recognition of sulphide by [CuL], Dalton Trans., 44(2015) 6490–6501.

[9] J. C. Qin, J. Yan, B. D. Wang, Z.Y. Yang, Rhodamine–naphthalene conjugate as a novel ratiometric fluorescent probe for recognition of Al^{3+}, Tetrahedron Lett., 57(2016) 1935–1939.

[10] Y. Yang, C.Y. Gao, T. Li, J. Chen, A Tetraphenylethene-Based Rhodamine Hydrazone Chemosensor for Colorimetric and Reversible Detection of Cu^{2+}, Chemistry Select,15 (2016) 4577-4581.

[11] A. Ghosh, A. Sengupta, A. Chattopadhyay, D. Das, A single probe for sensing both acetate and aluminum(III): visible region detection, red fluorescence and human breast cancer cell imaging, RSC Adv.,5 (2015) 24194-24199.

[12] A. Rai, A. K. Singh, A. K. Sonkar, A. Prakash, J. K. Roy, R. Nagarajan ,L. Mishra, A smart switchable module for the detection of multiple ions via turn-on dual-optical readout and their cell imaging studies, Dalton Trans., 45 (2016) 8272–8277.

[13] J. Hu, Z. Hu , Z. Chen , H. W. Gao , K. Uvdal, A logic gate-based fluorogenic probe for Hg(2+) detection and its applications in cellular imaging, Anal. Chim. Acta, 919 (2016) 85-93.

[14] A.Kumar, C.Kumari, D. Sain, S.K. Hira, P.P. Manna, S. Dey, Synthesis of Rhodamine-Based Chemosensor for Fe^{3+} Selective Detection with *off–on* Mechanism and its Biological Application in DL-Tumor Cells, Chemistry Select, 10 (2017) 2969-2974.

[15] Q.Hu, Y. Liu, Z. Li, R. Wen, Y. Gao, Y. Bei, Q. Zhu , A new rhodamine-based dual chemosensor for Al^{3+} and Cu^{2+}, Tetrahedron Lett., 55 (2014) 4912–4916

[16] L. Hou, J. Feng, Y. Wang, C. Dong, *S. Shuang, Y. Wang,* Single fluorescein-based probe for selective colorimetric and fluorometric dual sensing of Al^{3+} and Cu^{2+}, Sens Actuators B Chem, 247 (2017) 451-460; b)H. Kim, B.A. Rao , J.W. Jeong, S. Mallick, S.M. Kang, J.S.

Choi, C.S. Lee, Y.A. Son, A highly selective dual-channel Cu^{2+} and Al^{3+}chemodosimeter in aqueous systems: Sensing in living cells and microfluidic flows, *Sens Actuators B Chem*, 210 (2015) 173-182.

[17] a) C. Yu, J. Zhang, R. Wang , L. Chen, Highly sensitive and selective colorimetric and off-on fluorescent probe for Cu^{2+} based on rhodamine derivative, Org. Biomol. Chem., 8 (2010) 5277-5279 ; b)J. Fan, P. Zhan, M. Hu, W. Sun, J. Tang, J. Wang, S. Sun, F. Song , X. Peng, A Fluorescent Ratiometric Chemodosimeter for Cu^{2+} Based on TBET and Its Application in Living Cells, Org. Lett., 15 (2013) 492-495; c). M.C. Linder, M. H.Azam, Copper biochemistry and molecular biology, *Am. J. Clin. Nutr*. 63 (1996) 797S-811S.

[18] I. H. Scheinberg , A. G. Morell, *Inorganic Biochemistry ed* , (1973) 306–343.

[19] D. Strausak, J. F. B. Mercer, H. H. Dieter, W. Stremmel , G. Multhaup, Copper in disorders with neurological symptoms: Alzheimer's, Menkes, and Wilson diseases, Brain Res. Bull., 55 (2001) 175–185.

[20] D.R. Brown, H. Kozlowski, Biological inorganic and bioinorganic chemistry of neuro degeneration based on prion and Alzheimer diseases, Dalton Trans. 13 (2004) 1907–1917.

[21] S. Kim, J. Y. Noh, K. Y. Kim, J. H. Kim, H. K. Kang, S. W. Nam, S. H. Kim, S. Park, C. Kim , J. Kim, Salicylimine-Based Fluorescent Chemosensor for Aluminum Ions and Application to Bioimaging, Inorg. Chem., 51 (2012) 3597–3602.

[22] D.P. Perl, A.R. Brody, Alzheimer's disease: X-ray spectrometric evidence of aluminum accumulation in neurofibrillary tangle-bearing neurons, Science, 208 (1980) 297–299.

[23] E. Delhaize, P.R. Ryan, Aluminum Toxicity and Tolerance in Plants. Plant Physiol., 107 (1995) 315–321.

[24] D. Maity, T. Govindaraju, Conformationally Constrained (Coumarin−Triazolyl−Bipyridyl) Click Fluoroionophore as a Selective Al^{3+} Sensor, Inorg. Chem., 49 (2010) 7229–7231.

[25] S. Lee, K.K. Y. Yuen, K. A. Jolliffe, J. Yoon, Fluorescent and colorimetric chemosensors for pyrophosphate, Chem. Soc. Rev., 44 (2015) 1749—1762.

[26] F. Hide, M. A. Díaz-García, B. J. Schwartz, M. R. Andersson, Q. Pei, A. J. Heeger, Semiconducting Polymers: A New Class of Solid-State Laser Materials, Science, 273 (1996) 1833-1836.

[27] X. H.Zhu, J. B.Peng, Y. Caoa, J. Roncali, Solution-processable single-material molecular emitters for organic light-emitting devices,Chem. Soc. Rev., 40 (2011) 3509-3524.

[28] K. Kumar, H. Duan, R. S. Hegde, S. C. W. Koh, J. N. Wei, J. K. W. Yang, Printing colour at the optical diffraction limit, Nat .Nanotechnol., 7 (2012) 557-561.

[29] B.Yoon, J.Lee, I.S.Park, S. Jeon, J. Leea , J.M. Kim, Recent functional material based approaches to prevent and detect counterfeiting, J. Mater. Chem. C, 1 (2013) 2388-2403.

[30] (a) Y. Sagara, T. Kato, Mechanically induced luminescence changes in molecular assemblies, Nat. Chem., 1 (2009) 605-610; b)R.Diaz, E.Palleau, D.Poirot, N. M Sangeetha, L. Ressier, High-throughput fabrication of anti-counterfeiting colloid-based photoluminescentmicrotags using electrical nano imprint lithography, Nanotechnology , 25 (2014) 345302-345308.

[31] A. K. Singh, P. K. Yadav, N. Kumari, R. Nagarajan,L. Mishra, Alight/pH/multiple ion-driven smart switchable module for computing sequential logic operations *via* a resettable dual-optical readout, J. Mater. Chem. C, 3 (2015) 12123-12129.

[32] G.M.Sheldrick, SHELXS-97 Program for the Solution of Crystal Structures, University of Göttingen, Göttingen,Germany, 1997.

[33] G. M. Sheldrick, ActaCrystallogr.,Sect. A: Found. Crystallogr., 46 (1990) 467-473.

[34] M.J. Frisch, G.W. Trucks, G.E. Scuseria ,H.B. Schlegel, M.A. Robb, J.R. Cheeseman, V. Barone, G. Scalmani, B. Mennucci, G.A. Petersson, H. Nakatsuji, M. Caricato, X. Li, H.P. Hratchian, A.F. Izmaylov, J. Bloino, G. Zheng, J.L. Sonnenberg, M. Hada, M. Ehara, K. Toyota, R. Fukuda, J. Hasegawa, M. Ishida, T. Nakajima, Y. Honda, O. Kitao, H. Nakai, T. Vreven, J.A. Montgomery Jr., J.E. Peralta, F. Ogliaro, M. Bearpark, J.J. Heyd, E. Brothers, K.N. Kudin, V.N. Staroverov, R. Kobayashi, J. Normand, K. Raghavachari, A. Rendell, J.C. Burant, S.S. Iyengar, J. Tomasi, M. Cossi, N. Rega, J.M. Millam, M. Klene, G.A. Voth,J.E. Knox, J.B. Cross, V. Bakken, C. Adamo, J. Jaramillo, R. Gomperts, R.E. Stratmann, O. Yazyev, A.J. Austin, R. Cammi, C. Pomelli, J.W. Ochterski, R.L. Martin, K. Morokuma, V.G. Zakrzewski, , P. Salvador, J.J. Dannenberg, S. Dapprich, A.D. Daniels, O. Farkas, J.B. Foresman, J.V. Ortiz, J. Cioslowski, D.J. Fox, Gaussian 09, Revision A.02, Gaussian Inc., Wallingford, CT, 2009.

[35] M. M. Babu, NCI: A server to identify non-canonical interactions in protein structures,Nuc. Acids Res., 31 (2003) 3345-3348.

[36] A. Hakonen, Plasmon Enhancement and Surface Wave Quenching for Phase Ratiometry in Coextraction-Based Fluorosensors, Anal. Chem., 81 (2009) 4555-4559.

[37] H. A. Benesi and J. H. Hildebrand, A Spectrophotometric Investigation of the Interaction of Iodine with Aromatic Hydrocarbons. J. Am. Chem. Soc., 8 (1949) 2703-2707.